Physics – Uspekhi **58** (8) 819 – 827 (2015)

METHODOLOGICAL NOTES PACS numbers: 41.20.Jb, **41.60. – m**, 42.25.Bs, 61.80.Cb

Fresnel coefficients for parametric X-ray (Cherenkov) radiation

A V Shchagin

DOI: 10.3367/UFNe.0185.201508g.0885

Contents

Abstract. Parametric X-ray (Cherenkov) radiation (PXR) is considered to result from the crystal diffraction of virtual photons associated with a relativistic charged particle moving through the crystal. Formulas for PXR Fresnel coefficients are obtained in a kinematic approach, whose applicability is discussed. The derivation of the version of kinematic PXR theory using the Fresnel coefficients is described. By also using these coefficients, analytical expressions for the frequency, spectral peak width, differential yield by angles, and polarization of PXR are obtained and shown to compare well with the kinematic PXR theory of Ter-Mikaelian and with experimental PXR reflection studies.

Keywords: parametric X-ray radiation, Fresnel coefficients, virtual photons, crystal diffraction

1. Introduction

The Fresnel coefficients are usually considered and applied in real photon optics (see, for example, monograph [1]). Moreover, according to the Weizsacker–Williams method of equivalent photons [2], they can be used to describe the transformations of virtual photons associated with a moving charged particle into real photons. For example, in papers [3–5], Fresnel coefficients are derived for the transition radiation which is produced by a fast charged particle crossing the boundary between media with different dielectric constants.

Parametric X-ray radiation (PXR) occurs when a relativistic charged particle crosses a family of crystallographic planes in a crystal. M L Ter-Mikaelian devised a kinematic theory to describe PXR in a classical approximation (see equations (28.157)–(28.160) in book [6] and also review [7]). Ter-Mikaelian called this radiation 'resonant radiation' [6], but in the later literature the term 'parametric X-ray radiation' is used by an analogy to optical parametric Cherenkov radiation [8] which occurs when a charged particle crosses a medium consisting of periodically ordered layers with different dielectric constants. In the present paper, we will apply the term PXR, which is generally accepted in the modern literature.

The results of classical calculations [6] are confirmed by quantum calculations performed by H Nitta [9]. The fact that the kinematic theory can describe the basic properties of PXR emitted at large angles to the particle trajectory is also confirmed by many experiments (see, for example, reviews [10, 11] of such experiments). Let us note that, unlike conventional Vavilov–Cherenkov radiation, PXR is emitted if the particle speed is less than the phase velocity of the radiation propagation in the crystal.

Fresnel coefficients describing the diffraction of real photons in crystals were also discussed as a tool to describe PXR in Refs [11–13]. In this case, however, expressions for the Fresnel coefficients taking into account the properties of charged particles have not been derived yet. In the present paper, the analytical expressions for the Fresnel coefficients in the case of PXR are obtained. Moreover, we derive the expressions for the frequency and width of the spectral peak, differential yield (with respect to the angle) of PXR, and its polarization by using the Fresnel coefficients and compare

A V Shchagin Belgorod State National Research University, ul. Pobedy 85, 308015 Belgorod, Russian Federation;
National Science Center 'Kharkov Institute of Physics and Technology', ul. Akademicheskaya 1, 61108 Kharkov, Ukraine
E-mail: shchagin@kipt.kharkov.ua

Received 5 September 2014, revised 15 January 2015
Uspekhi Fizicheskikh Nauk **185** (8) 885 – 894 (2015)
DOI: 10.3367/UFNr.0185.201508g.0885
Translated by A L Chekhov; edited by A Radzig

these expressions with the predictions of the PXR kinematic theory and experimental results. We also discuss the conditions of the applicability of the kinematic approximation.

2. X-ray reflection from a single crystallographic plane

We assume that electromagnetic waves experience Thompson scattering on the electrons of the medium. Various methods for the derivation of absolute reflectance (Fresnel amplitude coefficient) for the X-rays reflecting from a single crystallographic plane are described, for example, in books [14, 15]. Fresnel amplitude coefficient (further, the Fresnel coefficient) $q_{\mathbf{g}}$ for the first-order reflection is described by the expression (see formulas (6.1) in Ref. [14] and (IV.3) in Ref. [15])

$$q_{\mathbf{g}} = -\mathrm{i}\,\frac{\lambda d A r_0}{v_\mathrm{c}\sin\phi}\,|S_{\mathbf{g}}|\,, \tag{1}$$

where λ is the X-ray radiation wavelength, d is the distance between crystallographic planes, $r_0 = e^2/(m_\mathrm{e}c^2) = 2.82\times10^{-13}$ cm is the classical electron radius, m_e is the electron mass, v_c is the volume of the crystal cell, ϕ is the angle between the propagation direction of the incident radiation and the crystallographic plane, $0 < \phi \leqslant \pi/2$, $S_{\mathbf{g}}$ is the structure amplitude of the crystallographic plane family which is described by the reciprocal lattice vector $\mathbf{g}$, $g = |\mathbf{g}| = 2\pi/d$, and Ar_0 is the scattering length [15]. The value of the factor A depends on the linear polarization direction of the incident radiation:

$$A_\perp = 1\,, \qquad A_\parallel = -\cos(2\phi)\,, \tag{2}$$

where $A_\perp$ and $A_\parallel$ are, respectively, factors for the radiation polarized perpendicularly and parallel to the diffraction plane. The diffraction plane goes through the propagation direction of the incident radiation and the vector $\mathbf{g}$.

Using the expressions (see, for example, equations (2.35) and (3.102) in book [16])

$$|S_{\mathbf{g}}| = \left|\chi_{\mathbf{g}}(\omega)\right|\frac{\pi v_\mathrm{c}}{\lambda^2 r_0} \tag{3}$$

and $\lambda = 2\pi c/(\omega\sqrt{\varepsilon}\,)$, we obtain the Fresnel coefficients (1) for the perpendicular and parallel polarizations as functions of the radiation angular frequency ω and the Fourier component of the crystal dielectric susceptibility $\chi_{\mathbf{g}}(\omega)$:

$$\begin{aligned} q_{\mathbf{g}\perp}(\omega) &= -\mathrm{i}\,\frac{\pi\omega\sqrt{\varepsilon}}{cg\sin\phi}\,\left|\chi_{\mathbf{g}}(\omega)\right|\,,\\ q_{\mathbf{g}\parallel}(\omega) &= \mathrm{i}\,\frac{\pi\omega\sqrt{\varepsilon}\cos(2\phi)}{cg\sin\phi}\,\left|\chi_{\mathbf{g}}(\omega)\right|\,, \end{aligned} \tag{4}$$

where c is the speed of light, and ε the dielectric constant. Let us note that the factors described by expressions (2) should be equal for axisymmetric backward diffraction, when $2\phi = \pi$. This confirms that the sign of $A_\parallel$ in formula (2) was chosen correctly.

3. Angular and spectral distributions of virtual photons associated with a relativistic charged particle traveling through a medium

Let us examine some properties of virtual photons that are associated with a charged particle which travels through a medium with constant velocity $\mathbf{V}$ and Lorentz factor $\gamma \gg 1$, where

$$\gamma = \frac{1}{\sqrt{1-(V/c)^2}}\,, \qquad V = |\mathbf{V}|\,.$$

The angular distribution J_v of normalized spectral density of virtual photons associated with a charged particle moving in a medium can be described by the formula (1.24) in book [12]. In the approximation of small angular deviations from the direction of the particle velocity $\mathbf{V}$ and in the conditions of $\gamma \gg 1$, $\hbar\omega \ll \gamma mc^2$, where m is the particle mass, the formula for angular distribution J_v has the form (see formula (4) in paper [17])

$$J_\mathrm{v} = \frac{\mathrm{d}N_\mathrm{v}}{\mathrm{d}\Omega\,\mathrm{d}\omega/\omega} = \frac{\alpha z^2}{\pi^2}\,\frac{\delta_{\mathrm{v}\perp}^2 + \delta_{\mathrm{v}\parallel}^2}{\left(\gamma_\mathrm{eff}^{-2} + \delta_{\mathrm{v}\perp}^2 + \delta_{\mathrm{v}\parallel}^2\right)^2}\,, \tag{5}$$

where $\mathrm{d}N_\mathrm{v}$ is the number of virtual photons in the solid angle $\mathrm{d}\Omega$, $\alpha = e^2/(\hbar c) \approx 1/137$ is the fine-structure constant, z is the particle charge in units of the electron charge $-e$, $\hbar$ is the Planck constant, $\delta_{\mathrm{v}\perp}, \delta_{\mathrm{v}\parallel} \ll 1$ are small angles between the direction of the radiation propagation and the direction of the particle velocity $\mathbf{V}$ in arbitrarily chosen perpendicular directions, $(\delta_{\mathrm{v}\perp}^2 + \delta_{\mathrm{v}\parallel}^2)^{1/2}$ is the angle between the vector $\mathbf{V}$ and the direction of the radiation propagation, $\gamma_\mathrm{eff} = (\gamma^{-2} + |\chi_0|)^{-1/2}$ is the effective relativistic factor [18] with due regard for Ter-Mikaelian longitudinal density effect [6, 7] (further, the density effect), χ_0 is the dielectric susceptibility for the radiation frequency ω higher than the frequencies of the atomic transitions and off the resonance frequencies, $|\chi_0| = 1 - \varepsilon = (\omega_\mathrm{p}/\omega)^2$, where ε is the mean dielectric constant, and ω_p is the plasma frequency of the medium. Let us also note that the phase velocity of the X-ray propagation in the medium is usually higher than the speed of light, $c/\sqrt{\varepsilon} > c$, because $\varepsilon < 1$.

One can see from expression (5) that the virtual photons are symmetrically distributed around the velocity vector of the particle $\mathbf{V}$. The maximum of the distribution is resided at the angle γ_eff^{-1} to the particle's velocity vector $\mathbf{V}$, and there is a dip in the center of the distribution, so if $\delta_{\mathrm{v}\perp}, \delta_{\mathrm{v}\parallel} = 0$, the number of virtual photons is zero. In order to obtain the distribution of virtual photons for a particle traveling in a vacuum, one should replace γ_eff in expression (5) with γ. The angular distribution of virtual photons broadens as the particle goes from the vacuum to the medium and narrows as it leaves the medium, because $\gamma_\mathrm{eff}^{-1} > \gamma^{-1}$. The restructuring of the particle field is accompanied by the emergence of transition radiation [3–5], and formula (5) describes the distribution in a stationary state.

The spectral distribution of virtual photons does not have any peculiarities. One can see from formula (5) that the number of virtual photons propagating in any direction per unit frequency interval monotonically decreases as the frequency increases: $\mathrm{d}N_\mathrm{v}/(\mathrm{d}\Omega\,\mathrm{d}\omega) \sim 1/\omega$.

4. Emission of parametric X-ray radiation from a crystal

We will consider the diffraction of virtual photons — that is, the emission of real PXR quanta when a charged particle with the relativistic factor $\gamma \gg 1$ passes through a family of crystallographic planes, which is characterized by the reciprocal lattice vector $\mathbf{g}$. The number $\mathrm{d}N_\mathrm{PXR}$ of PXR quanta emitted into the solid angle $\mathrm{d}\Omega$ as the particle

passes through M crystallographic planes can be expressed in the kinematic approximation using the interference function $I = \sin^2(Mx)/\sin^2 x$ [1, 15], where the variable x is described by expressions (8), (9) from Section 5 in the following form:

$$Y_{\mathrm{PXR}} = \frac{\mathrm{d}N_{\mathrm{PXR}}}{\mathrm{d}\Omega} = \int\left[\left|q_{\mathbf{g}\perp}(\omega)\right|^2 I(x)\, J_{\mathrm{v}\perp} + \left|q_{\mathbf{g}\parallel}(\omega)\right|^2 I(x)\, J_{\mathrm{v}\parallel}\right]\frac{\mathrm{d}\omega}{\omega}\,. \tag{6}$$

Here, $J_{\mathrm{v}\perp}$ and $J_{\mathrm{v}\parallel}$ are the distributions of virtual photons with, respectively, perpendicular and parallel polarizations in the small-angle approximation:

$$J_{\mathrm{v}\perp} = \left(\frac{\mathrm{d}N_{\mathrm{v}}}{\mathrm{d}\Omega\,\mathrm{d}\omega/\omega}\right)_{\perp} = \frac{\alpha z^2}{\pi^2}\frac{\delta_{\mathrm{v}\perp}^2}{\left(\gamma_{\mathrm{eff}}^{-2} + \delta_{\mathrm{v}\perp}^2 + \delta_{\mathrm{v}\parallel}^2\right)^2}\,,$$
$$J_{\mathrm{v}\parallel} = \left(\frac{\mathrm{d}N_{\mathrm{v}}}{\mathrm{d}\Omega\,\mathrm{d}\omega/\omega}\right)_{\parallel} = \frac{\alpha z^2}{\pi^2}\frac{\delta_{\mathrm{v}\parallel}^2}{\left(\gamma_{\mathrm{eff}}^{-2} + \delta_{\mathrm{v}\perp}^2 + \delta_{\mathrm{v}\parallel}^2\right)^2}\,, \tag{7}$$

where $\delta_{\mathrm{v}\perp}, \delta_{\mathrm{v}\parallel} \ll 1$ are the small angles with respect to the charged particle velocity $\mathbf{V}$ in planes perpendicular and parallel to the diffraction plane, respectively. In the case of PXR, by the diffraction plane is meant the plane in which the reciprocal lattice vector and the particle velocity vector lie. The full number of virtual photons is expressed by the sum $J_{\mathrm{v}} = J_{\mathrm{v}\perp} + J_{\mathrm{v}\parallel}$ [see formula (5)].

If we apply the kinematic approximation, we only consider the radiation emitted by the particle, and reflections of the radiation on the crystallographic planes are not taken into account.

5. Spectral peak frequency of parametric X-ray radiation

The interference function in formula (6) describes the spectral properties of PXR. The quantity x is half the phase difference between the radiation emitted from adjacent crystallographic planes [1, 15]: $x = 2\pi(a/\lambda)/2$. For PXR, this quantity can be found from Fig. 1 by utilizing the path difference between two wavefronts:

$$a = \frac{d}{\sin\phi}\left(\frac{c}{V\sqrt{\varepsilon}} - \cos\theta\right),$$

where ϕ is the angle between the particle velocity vector and the crystallographic plane.

Taking into account the relation $\lambda = 2\pi c/(\omega\sqrt{\varepsilon})$, we obtain

$$x = \frac{\pi\omega}{gV\sin\phi}\left(1 - \frac{V\sqrt{\varepsilon}}{c}\cos\theta\right). \tag{8}$$

The first-order peak of the interference function corresponds to $x = \pi$. Therefore, we can write out the expression

$$x = \frac{\pi\omega}{\omega_{\mathrm{PXR}}} \tag{9}$$

and find, using formulas (8) and (9), the frequency ω_{PXR} of the PXR first-order spectral peak:

$$\omega_{\mathrm{PXR}} = \frac{gV\sin\phi}{1 - (V\sqrt{\varepsilon}/c)\cos\theta}\,. \tag{10}$$

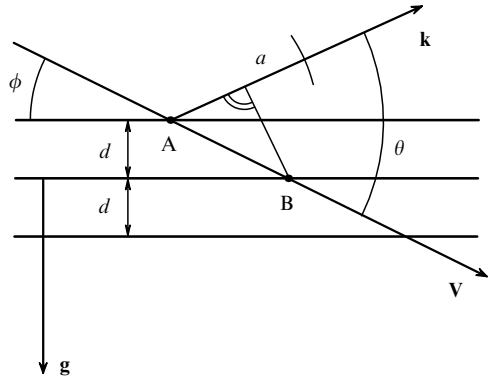

Figure 1. Particle with a constant velocity **V** crosses a family of crystallographic planes at the angle ϕ and emits radiation with the wave vector **k** at the angle θ with respect to the vector **V**. Crystallographic planes with spacing d are characterized by the reciprocal lattice vector **g**. The region of the spherical wavefront of the radiation emitted from the point A (shown as an arc on the **k** vector at the moment when the particle reaches the point B) is ahead of the wavefront emitted from the point B. The distance between them is $a = (c/\sqrt{\varepsilon})\Delta t - d\cos\theta/\sin\phi$, where $\Delta t = d/(V\sin\phi)$ is the time which the particle takes to pass the distance between adjacent crystallographic planes — that is, from point A to point B.

Expression (10) was first derived in monograph [6] [see Eqns (28.6) and (28.158)] from the energy and momentum conservation laws. Moreover, frequency (10) can be obtained from the Huygens scheme for PXR, proposed in book [10] (see also book [20]).

One of the remarkable properties of PXR lies with the ability to gradually tune the frequency of the PXR spectral peak by simply rotating the crystal target placed in a beam of accelerated particles, i.e. correspondingly changing the angle ϕ in formula (10). Gradual tuning of the PXR spectral peak frequency has been observed in various experiments in the energy range of PXR quanta from several keV [18, 19] up to 400 keV [21]. The cited articles experimentally confirm the validity of expression (10).

6. Spectral peak width of parametric X-ray radiation

Using formula (9), we can express the interference function in the form

$$I = \frac{\sin^2(M\pi\omega/\omega_{\mathrm{PXR}})}{\sin^2(\pi\omega/\omega_{\mathrm{PXR}})}\,. \tag{11}$$

The maximum value of function (11) at the peak, when $\omega = \omega_{\mathrm{PXR}}$, equals M^2. In order to define the full width at half maximum (FWHM) of the PXR spectral peak, two solutions, ω_1 and ω_2, of the transcendent equation

$$I = \frac{M^2}{2} \tag{12}$$

and their difference $\Delta\omega = \omega_2 - \omega_1$ must be found. As a result, we obtain the normalized FWHM of the PXR spectral peak:

$$\frac{\Delta\omega}{\omega_{\mathrm{PXR}}} = 0.89\,M^{-1}\,. \tag{13}$$

Let us note that in paper [6] the radiation emission from an infinite crystal was considered and, instead of the

interference function, the delta function was used. Therefore, the width of the PXR spectral peak in Ref. [6] equals zero.

Formula (13) with a coefficient equal to unity is present in Ref. [12]. The result (13) was also obtained in Ref. [22], where PXR emitted from a finite transparent crystal was simply considered as a constant amplitude wave train. The number of oscillations in the train was equal to the number of crystallographic planes M which the particle crossed.

Note that the expression for the normalized FWHM of the PXR spectral peak (13) was obtained for ideal conditions, without taking into account the effects of particle multiple scattering in the crystal, the radiation attenuation in the crystal itself, or the experimental angular resolution. Therefore, expression (13) holds true only in the case of relatively thin transparent crystals and ideal angular resolution. Changing these conditions can lead to the broadening of the PXR spectral peak.

The influence of the real experimental angular resolution, the experiment geometry, and the radiation attenuation on the width of the PXR spectral peak was studied in Refs [19, 23], and the influence of particle multiple scattering was looked at in paper [24]. A typical value for the normalized FWHM of the PXR spectral peak in the experiment with a thin crystal is on the order of 10^{-2} [19], and a minimal normalized width of up to $\sim 10^{-9}$ can be obtained by generating focused PXR from a particle moving in a channeling regime through a long bent crystal [25] (see also Ref. [26]). In this case, the length of the PXR wave train can reach several centimeters [25]. This means that the answer to the question, stated in the title of paper [23] "How narrow is the linewidth of parametric X-ray radiation?" can be found in Ref. [25].

7. Fresnel coefficients for parametric X-ray radiation

In order to find the PXR yield, we will remove the functions which vary slowly in the vicinity of the frequency $\omega = \omega_{\mathrm{PXR}}$ from under the integral in formula (6):

$$Y_{\mathrm{PXR}} = \frac{\mathrm{d}N_{\mathrm{PXR}}}{\mathrm{d}\Omega} = \left(\left|q_{\mathbf{g}\perp}(\omega_{\mathrm{PXR}})\right|^2 J_{\mathrm{v}\perp} + \left|q_{\mathbf{g}\parallel}(\omega_{\mathrm{PXR}})\right|^2 J_{\mathrm{v}\parallel}\right) \times \int \frac{\sin^2(M\pi\omega/\omega_{\mathrm{PXR}})}{\sin^2(\pi\omega/\omega_{\mathrm{PXR}})} \frac{\mathrm{d}\omega}{\omega_{\mathrm{PXR}}} . \tag{14}$$

The integral on the right-hand side of formula (14), taken over the frequency region around the spectral peak at $\omega = \omega_{\mathrm{PXR}}$, equals the number of crystallographic planes M [15]. Therefore, we can write out the expression

$$Y_{\mathrm{PXR}} = \frac{\mathrm{d}N_{\mathrm{PXR}}}{\mathrm{d}\Omega} = |F_\perp|^2 J_{\mathrm{v}\perp} + |F_\parallel|^2 J_{\mathrm{v}\parallel} , \tag{15}$$

where $F_\perp$ and $F_\parallel$ are the Fresnel coefficients for PXR with perpendicular and parallel polarizations, respectively:

$$F_\perp = \sqrt{M} q_{\mathbf{g}\perp}(\omega_{\mathrm{PXR}}) = -\mathrm{i}\,\frac{\sqrt{M}\pi\left|\chi_{\mathbf{g}}(\omega_{\mathrm{PXR}})\right|}{c/(V\sqrt{\varepsilon}) - \cos\theta} ,$$
$$F_\parallel = \sqrt{M} q_{\mathbf{g}\parallel}(\omega_{\mathrm{PXR}}) = \mathrm{i}\,\frac{\sqrt{M}\pi\left|\chi_{\mathbf{g}}(\omega_{\mathrm{PXR}})\right|\cos(2\phi)}{c/(V\sqrt{\varepsilon}) - \cos\theta} . \tag{16}$$

Fresnel coefficients (16) depend not only on the geometry and properties of the crystal, but also on the velocity of motion of the charged particle. Note that these coefficients are related to the PXR spectral peak integrated over the frequency.

8. Differential yield of parametric X-ray radiation

By substituting formulas (7) and (16) into expression (15), we obtain the relationship for the differential (with respect to the angles) yield of PXR:

$$Y_{\mathrm{PXR}} = \frac{\mathrm{d}N_{\mathrm{PXR}}}{\mathrm{d}\Omega} = \frac{\alpha z^2 M\left|\chi_{\mathbf{g}}(\omega_{\mathrm{PXR}})\right|^2}{\left[c/(V\sqrt{\varepsilon}) - \cos\theta\right]^2} \frac{\delta_\perp^2 + \delta_\parallel^2\cos^2(2\phi)}{(\gamma_{\mathrm{eff}}^{-2} + \delta_\perp^2 + \delta_\parallel^2)^2} , \tag{17}$$

where the radiation frequency ω_{PXR} is described by expression (10), and $\delta_\perp$, $\delta_\parallel \ll 1$ are the small angles that define the direction of the radiation propagation with respect to the direction of the PRX reflection center. The angles $\delta_\perp$, $\delta_\parallel$ are measured in the directions perpendicular and parallel to the PXR diffraction plane, respectively. The PXR diffraction plane goes through the vectors $\mathbf{V}$ and $\mathbf{g}$. The angle between the velocity of the particles $\mathbf{V}$ and the PXR reflection center equals 2ϕ in the diffraction plane, $\theta = 2\phi - \delta_\parallel$, and M is the number of crystallographic planes which contribute to the formation of PXR reflection. In a crystal which is transparent at frequencies ω_{PXR}, M is simply the number of crystallographic planes crossed by the moving particle. In the case of an absorbing crystal, M decreases due to the attenuation of the radiation in the crystal. The effective number of crystallographic planes which contribute to the formation of PXR reflection in this case can be found using the following expression (see, for example, formulas (13), (14) in paper [27]):

$$M = \frac{T_{\mathrm{e}}}{2\pi}\left|\mathbf{g}\mathbf{v}\,\frac{\mathbf{t}\boldsymbol{\Omega}}{\mathbf{t}\mathbf{v}}\right|\left[1 - \exp\left(-\frac{T}{T_{\mathrm{e}}|\mathbf{t}\boldsymbol{\Omega}|}\right)\right] , \tag{18}$$

where $\mathbf{t}$ is the unit vector perpendicular to the plate surface, $\boldsymbol{\Omega}$ is the unit vector in the direction of radiation propagation, $\mathbf{v} = \mathbf{V}/V$ is the unit vector in the direction of the particle motion, T is the thickness of the crystal plate, T_{e} is the path length at which radiation with the frequency ω_{PXR} attenuates by a factor of e: $T_{\mathrm{e}} = 1/\mu$, where μ is the attenuation coefficient for the radiation in the crystal.

As follows from formula (17), the maximum PXR yield is expected at the angle $\eta = \gamma_{\mathrm{eff}}^{-1}$, where $\eta = (\delta_\perp^2 + \delta_\parallel^2)^{1/2}$ is the angle of deflection from the reflection center in an arbitrary direction. The region of the angular distribution with $\eta \sim \gamma_{\mathrm{eff}}^{-1}$ is called the PXR reflection, and the angle $\gamma_{\mathrm{eff}}^{-1}$ is the angular size of the PXR reflection. In the center of the PXR reflection one can observe a dip where the radiation yield decreases to zero at $\delta_\perp$, $\delta_\parallel = 0$. The shape of the angular distribution for the number of real photons in the PXR reflection (17) is similar to that for the number of virtual photons of the particle (5), but the coefficients in formula (17) are different for different directions of radiation polarization. It can be said that the PXR reflection is reflection of the distribution for virtual photons (5) at frequency ω_{PXR} with the radiation polarization taken into account. A typical schematic for the generation of the PXR reflection is shown in Fig. 2.

Expression (17) coincides with the expression which was obtained in the framework of the Ter-Mikaelian theory in the small-angle approximation (see formulas (15), (22) in

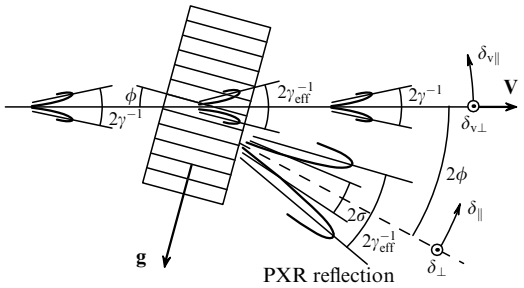

Figure 2. Typical schematic of PXR reflection generation, shown in the diffraction plane. Angular coordinates $\delta_{v\perp}, \delta_{\perp}$, which are measured in the directions perpendicular to this plane, are marked by circles with dots. A charged particle moves with the constant velocity **V** in vacuum and crosses the crystal plate. One of the crystallographic planes of the crystal with a nonzero structure factor, shown by the dashed line, is characterized by the reciprocal lattice vector **g**. Angular distributions for the number of virtual photons of the particle in a stationary state are depicted by diagrams at different sections of the particle trajectory: distribution in the crystal (5) with a maximal number of virtual photons at angles $\delta_{v\perp}, \delta_{v\parallel} = \pm\gamma_{eff}^{-1}$, and distribution in the vacuum (5), before the particle enters and after it leaves the crystal, with the quantity γ^{-1} instead of γ_{eff}^{-1} and a maximal number of virtual photons at angles $\delta_{v\perp}, \delta_{v\parallel} = \pm\gamma^{-1}$; ϕ is the angle between the crystallographic planes and the vector **V**. The PXR reflection is emitted at the angle 2ϕ to the vector **V**. Angular distribution for the yield of the real photons in PXR reflection (17) is shown by the diagram; the maximal yield in the PXR reflection is found in the direction at the angles $\delta_{\perp}, \delta_{\parallel} = \pm\gamma_{eff}^{-1}$ to the direction of the reflection center, shown by the dashed line. The angular region 2σ (31) is also indicated as the one where strong effects associated with the PXR dynamical diffraction are possible.

Ref. [17]) up to a factor

$$\varepsilon^{7/2}\left(\frac{V}{c}\right)^2 \approx \left[1-\left(\frac{\omega_p}{\omega}\right)^2\right]^{7/2}(1-\gamma^{-2})\,.$$

In the case of X-ray radiation and for $\gamma \gg 1$, this factor is almost equal to unity. For example, $\varepsilon^{7/2} \approx 1-3.3\times10^{-5}$ in a single-crystalline Si at $\hbar\omega = 10$ keV and $(V/c)^2 = 1-1.0\times10^{-4}$ for electrons with an energy of 50 MeV. Moreover, expression (17) is similar to the expressions obtained in the framework of other versions of PXR kinematic theory, which are discussed in paper [28].

The kinematic theory with the aid of expression (17) rather well describes the experimentally observed PXR yield in the regions of reflection maxima and at angular distances from its center of up to ten PXR reflection angular sizes (see, for example, Refs [18, 29, 30]). At the same time, a comparison of PXR theory predictions with experimental results in the vicinity of the reflection center is difficult, because there are other types of radiation as well. For example, one can find in the vicinity of the reflection center diffraction maxima of the bremsstrahlung emitted by a particle in the crystal and of the transition radiation which is generated as the particle enters the crystal. The intensity of these types of radiation can be much higher than the PXR intensity near the reflection center. For example, the radiation yield in the reflection center observed in experiments [18, 29] was only about half of that in the reflection maxima, in contrast to the dip close to the zero value predicted by the PXR kinematic theory [see formula (17)]. This means that the PXR yield is masked by other types of radiation in the region of the reflection center.

One of the features of the Ter-Mikaelian theory consists in the prediction of asymmetry of the radiation yield in the PXR reflection with respect to its center for an arbitrarily large energy of the incident particles. Recently, this prediction was verified in paper [27]. The theory was compared with the experimental data obtained with a high angular resolution under the condition of $\gamma^{-2} < |\chi_0|$ [29], when the PXR yield is suppressed due to the density effect [for incident electrons with high energy (255 MeV)] and under the condition of $\gamma^{-2} > |\chi_0|$ [18], when the influence of the density effect is negligible (for moderate energies of the incident electrons, 15.7 and 25.7 MeV). The comparison showed good agreement of the experimentally observed asymmetry in the PXR reflection emitted in the front hemisphere with the one calculated using expressions (15), (22) from paper [17], which almost coincide with expression (17) obtained in this paper. The asymmetry in formula (17) can be clearly seen with the relation $\theta = 2\phi - \delta_{\parallel}$ taken into account.

The absolute differential yield in the maxima of the PXR reflection observed in experiments with a thin silicon crystal, is, for example, on the order of 2×10^{-4} quanta per electron per sr at an electron energy of 25.7 MeV [18], and on the order of 5×10^{-3} quanta per electron per sr at an electron energy of 855 MeV [28]. Crystals consisting of light elements are the most suitable for the generation of PXR reflections [31]. A two-dimensional image of the angular distribution for the yield of the quanta in PXR reflection was first observed in Ref. [32], and it was measured with a high angular resolution in Ref. [29]. The calculated results for the structure of the differential yield in PXR reflections emitted under different angles in the front and rear hemispheres are presented in diagrams in papers [26, 33].

Above, we only discussed the first-order PXR spectral peaks at the frequency ω_{PXR} (10). PXR can also be generated at multiple frequencies but not for any multiplicity. PXR reflection exists if the structure factor of the crystallographic plane is nonzero. For example, PXR can be generated at single frequency on crystallographic (111) planes, and at triple frequency on (333) planes of a crystal with a diamond structure, but PXR cannot be generated at the double frequency on (222) planes due to the zero value of the structure factor for the (222) plane. This condition can be considered an analog to the condition that the real X-ray radiation can be reflected from the crystal.

In the case of several PXR reflections, the total radiation yield Y is calculated with the expression

$$Y = \sum_{\mathbf{g}} Y_{PXR}\,, \tag{19}$$

where the summation is performed over planes with nonzero structure factors.

One can see from expression (17) that for moderate energies of the incident particles, given by $\gamma^2 \ll 1/|\chi_0|$, the radiation yield in the PXR reflection maxima increases as the square of the particle energy, whereas the angular size of the reflection is inversely proportional to the particle energy. The influence of the density effect leads to the fact that distribution (17) ceases to depend on the energy of the incident particles altogether, once their energy is high enough for the condition $\gamma^2 \gg 1/|\chi_0|$ to be fulfilled. The change in the behavior of differential yield (17) takes place in the region of the particle energies corresponding to the critical energy described by the condition $\gamma_{crit} = 1/\sqrt{|\chi_0|}$ [10, 18]. For example, if PXR with an energy of $\hbar\omega_{PXR} = 12.9$ keV is

emitted by electrons in a silicon crystal, the critical energy of the electrons is 212 MeV. The physical reason for the density effect is connected with the similar behavior of distribution (5) for the virtual photons in the medium, which are the source of the PXR.

9. Linear polarization of radiation in the PXR reflection

It is well known that virtual photons are linearly polarized in radial directions with respect to the particle's velocity. PXR reflection is formed as a result of the diffraction of polarized virtual photons. Therefore, the differential (with respect to the angles) yield in the PXR reflection should be linearly polarized as well.

Following the methods of paper [34], we will describe the linear polarization direction in the PXR reflection by the angle ρ between the radiation polarization plane (the plane going through the wave vector and the electric field vector) and the diffraction plane. The tangent of the angle ρ is equal to the ratio between the perpendicular ($E_\perp$) and parallel ($E_\parallel$) components of the electric field. Taking into account the Fresnel coefficients (16) and the small-angle approximation, we obtain

$$\tan\rho = \frac{E_\perp}{E_\parallel} = \frac{F_\perp\sqrt{J_{\mathrm{v}\perp}}}{F_\parallel\sqrt{J_{\mathrm{v}\parallel}}} = -\frac{\delta_\perp}{\delta_\parallel\cos(2\phi)}\,. \tag{20}$$

Expression (20) can be considered a differential equation for the curves $\delta_\perp = \delta_\perp(\delta_\parallel)$, which are tangent to the direction of the electric field vector (to the direction of the linear radiation polarization) at every point:

$$\frac{\mathrm{d}\delta_\perp}{\mathrm{d}\delta_\parallel} = -\frac{\delta_\perp}{\delta_\parallel\cos(2\phi)}\,. \tag{21}$$

After solving equation (21), we obtain a set of curves with an arbitrary constant B:

$$\delta_\perp = B|\delta_\parallel|^{-1/\cos(2\phi)}\,, \tag{22}$$

which describe the polarization structure of the PXR reflection.

Note that the sign of the phase of the Fresnel coefficient $F_\perp$ (16) for PXR with a perpendicular polarization does not depend on the angle ϕ. At the same time, the sign of the phase of the Fresnel coefficient $F_\parallel$ (16) for PXR with a parallel polarization and the sign of the exponent in expression (22) change in the vicinity of the reflection emission angle $2\phi = \pi/2$. This leads to a significant difference in the structures of the linear polarization (22) in the PXR reflections emitted in the front and rear hemispheres. In the case of PXR reflection emitted in the front hemisphere for $2\phi < \pi/2$, curves (22), which are tangent to the directions of the linear polarization, have a hyperbolic form, while in the case of emission in the rear hemisphere, $2\phi > \pi/2$, these curves are parabolic.

The calculated results for the structure of the linear polarization in PXR reflections emitted at various angles in the front and rear hemispheres are present in Fig. 2 in paper [34], as well as in figures plotted in papers [26, 33]. The calculated results are in good agreement with the results of the lab measurements of the PXR polarization performed by Morokhovskii et al. [35].

10. Applicability of the kinematic approximation for describing the parametric X-ray radiation reflection

PXR is emitted by a particle traveling through a crystal, while the frequency and propagation direction of the radiation in the PXR reflection are close to the conditions for the diffraction of the radiation in the crystal. Soon after the kinematic theory was published [6], the dynamical theory of PXR was put forward in papers [36, 37], where the dynamic diffraction of the PXR in the crystal was taken into account. According to the dynamic theory, the radiation from the PXR reflection undergoes diffraction in the same family of crystallographic planes which it was generated from, and the diffracted radiation can be emitted in the forward direction, near the particle velocity vector $\mathbf{V}$.

Later on, experiments at accelerators showed that the radiation registered in the PXR reflection had properties which were well described by the kinematic theory (see, for example, Refs [10, 11, 28–30]), but no radiation diffracted in the forward direction was observed. At the same time, discussions on the nature and possibility of the existence and observation of PXR generated in the forward direction continued (see, for example, Refs [7, 38–40] and a brief review of these discussions in paper [41]). At last, narrow spectral peaks of the diffracted PXR were experimentally observed in a narrow angular region around the particle velocity vector $\mathbf{V}$ [41, 42]. Further, we will discuss the conditions under which the PXR diffraction becomes significant, and the conditions under which the kinematic approximation is valid.

The frequency (10) of the PXR spectral peak slightly differs from the Bragg frequency ω_B in the crystal:

$$\omega_\mathrm{B} = \frac{cg^2}{2\sqrt{\varepsilon}\,|\boldsymbol{\Omega}\mathbf{g}|}\,, \tag{23}$$

where $\boldsymbol{\Omega}$ is the unit vector in the direction of PXR propagation. The explicit expression for the normalized difference between the Bragg (23) and PXR (10) frequencies in the small-angle approximation of $\delta_\perp, \delta_\parallel \ll 1$ near the PXR reflection center was obtained in paper [43]:

$$\frac{\omega_\mathrm{B} - \omega_\mathrm{PXR}}{\omega_\mathrm{PXR}} \approx \frac{\gamma^{-2} + |\chi_0| + \eta^2}{4\sin^2\phi} = \frac{\gamma_\mathrm{eff}^{-2} + \eta^2}{4\sin^2\phi}\,, \tag{24}$$

where $\eta = (\delta_\perp^2 + \delta_\parallel^2)^{1/2}$ is the angle of deflection from the reflection center in an arbitrary direction. One can see from the last formula that the PXR frequency is always lower than the Bragg frequency, and the frequency difference is minimal in the region of the reflection center, at $\eta = 0$, where the PXR yield is close to zero according to formula (17). In the region of the PXR reflection, where the radiation yield is maximal and $\eta = \gamma_\mathrm{eff}^{-1}$, the frequency difference (24) can be expressed as $\gamma_\mathrm{eff}^{-2}/(2\sin^2\phi)$. The frequency difference (24) rapidly increases with a further increase in the angle of deflection η from the PXR reflection center.

It is well known that dynamic diffraction effects can be significant in the crystal when the monochromatic ray of Röntgen radiation is deflected from the exact Bragg propagation direction by not more than for the angle

$$\Delta\vartheta = \pm\frac{C\,|\chi_g|}{\sin(2\phi)}\,, \tag{25}$$

where the factor $C = 1$ for the perpendicular polarization of the radiation (σ-polarization), and $C = |\cos(2\phi)|$ for the parallel one (π-polarization). Beyond these limits, the effects associated with the dynamic diffraction rapidly weaken [16]. In our case of radiation with a fixed propagation direction, the corresponding deviation limits of the radiation frequency from the Bragg frequency can easily be found by differentiating the Bragg law. The limits are expressed as

$$\frac{\Delta\omega_{\rm B}}{\omega_{\rm B}} = \pm\frac{C|\chi_g|}{2\sin^2\phi}\,. \tag{26}$$

By comparing formulas (24) and (26), we can estimate the conditions under which the dynamic diffraction effects become significant for PXR. Obviously, it is possible when the PXR frequency deviation (24) lies within the limits (26) — that is, when

$$\frac{(\omega_{\rm B}-\omega_{\rm PXR})/\omega_{\rm PXR}}{|\Delta\omega_{\rm B}/\omega_{\rm B}|} \leqslant 1\,. \tag{27}$$

By substituting expressions (24) and (26) into (27), we obtain an estimate for the angular size $\sigma_{\rm D}$ of the region around the PXR reflection center, where the effects associated with PXR dynamic diffraction can be strongly pronounced:

$$\eta \leqslant \sigma_{\rm D} = \gamma_{\rm eff}^{-1}\sqrt{\frac{2C\,|\chi_g|}{\gamma_{\rm eff}^{-2}} - 1}\,. \tag{28}$$

The condition that this angle really exists corresponds to the positive sign of the radicand in formula (28):

$$2C\,|\chi_g| > \gamma_{\rm eff}^{-2}\,. \tag{29}$$

It is interesting to note that the condition (29) for the PXR diffraction to exist and the angular size (28) of the region near the PXR reflection center, where the diffraction is possible, do not depend on the emission direction for the PXR reflection.

Now let us consider the most favorable case of the sufficiently high energy of the incident particles for the dynamical effects to be pronounced, when the value of γ^{-2} can be neglected, since it is small in comparison with $|\chi_0|$, and so the density effect is strongly pronounced:

$$\gamma^{-2} \ll |\chi_0|\,. \tag{30}$$

In this case, the angular size $\gamma_{\rm eff}^{-1} = \sqrt{|\chi_0|}$ of the PXR reflection ceases to depend on the incident particle energy any more and an estimate of the angular size σ (28) of the central region becomes dependent only on the crystal properties and PXR polarization:

$$\eta \leqslant \sigma = \sqrt{|\chi_0|}\sqrt{\frac{2C|\chi_g|}{|\chi_0|} - 1}\,, \tag{31}$$

and condition (29) takes the form

$$2C\,|\chi_g| > |\chi_0|\,. \tag{32}$$

Note that the inequality $\sigma > \sigma_{\rm D}$ always holds true. The position of the reflection central region with the angular size σ is shown in Fig. 2. The angular size (31) of the region can be expressed in (normalized to) units of the angular size of the PXR reflection:

$$\sigma_{\rm N} = \frac{\sigma}{\sqrt{|\chi_0|}} = \sqrt{\frac{2C\,|\chi_g|}{|\chi_0|} - 1}\,. \tag{33}$$

Inequalities (29) and (32) can be considered as criteria for the choice of the crystallographic planes on which the dynamic diffraction is possible, while expressions (28), (31), and (33) can be utilized to estimate the angular sizes of the region around the PXR reflection center, where the dynamic diffraction can be pronounced. Additionally, less pronounced effects of dynamic diffraction and enhanced attenuation of the radiation could be observed near the boundaries (28), (31), (33) of the region, and the side peaks of the pendulum type solution can appear near this region in the case of thin crystals.

Further, we will discuss the case of perpendicular polarization, when $C = 1$, in more detail. In this case, as was mentioned above, the condition (32) for the PXR diffraction to exist and the angular size (33) of the central region depend only on the crystal properties:

$$2|\chi_g| > |\chi_0|\,, \tag{34}$$

$$\sigma_{\rm N} = \frac{\sigma}{\sqrt{|\chi_0|}} = \sqrt{\frac{2|\chi_g|}{|\chi_0|} - 1}\,. \tag{35}$$

The most popular crystal for PXR experiments is the single-crystal silicon; therefore, we will make estimations regarding this crystal. The calculations show that at PXR frequencies higher than the atomic transition frequencies and off the resonance frequencies condition (34) is fulfilled only for three crystallographic planes with a nonzero structure factor: (111), (220), and (400), and the angular size $\sigma_{\rm N}$ (35) of the region is 0.275, 0.45, and 0.077 times the angular size of the PXR reflection, respectively. This means that only a small central angular part of the PXR reflections, where the radiation yield is minimal, can effectively undergo diffraction. Condition (34) is not fulfilled for other silicon crystallographic planes.

A similar situation takes place in the case of a germanium crystal, where the angular size $\sigma_{\rm N}$ (35) of the region is 0.47, 0.67, 0.45, and 0.18 for crystallographic planes for which the structure factor is nonzero and condition (34) is fulfilled; these are planes (111), (220), (400), and (422), respectively. The dynamic PXR diffraction should be most pronounced for the crystallographic plane (220) in both crystals. The cases of other crystals need additional analysis.

Experiments on the observation of the two-dimensional angular distribution for the PXR reflection yield were performed in the case of a silicon crystal and the crystallographic plane (220) in papers [29, 32]. In these experiments, the basic properties of the reflection were well described by the kinematic theory of PXR and there was no need to consider the dynamic diffraction. However, this does not exclude the possibility of some part of the radiation from the PXR reflection central region being diffracted in the forward direction.

Radiation from PXR reflection, diffracted on the (111) crystallographic plane of a single-crystal silicon, was observed in Ref. [41]. The radiation was observed in the forward direction in the angular region, where the deviation angle from the particle's velocity vector direction was not more than approximately $\pm 0.36\sqrt{|\chi_0|}$ (see Fig. 3 in paper

[41]). These angles are close to the estimate $\pm 0.275\sqrt{|\chi_0|}$ we have obtained above for the boundaries of the angular region for this crystallographic plane.

It is obvious that the kinematic theory is not able to describe the properties of PXR diffracted in the forward direction, which was observed in Refs [41, 42]. Effects associated with dynamic diffraction can be poorly pronounced in the central region of the PXR reflection, due to low PXR intensity in this region and the masking influence of other types of diffracted radiation, as discussed in Section 8. Therefore, the dynamic diffraction of the PXR is poorly pronounced in experimental observations of the PXR reflections, and the properties of the reflection are well described by the kinematic theory.

Let us note that, although the frequency of the PXR in the reflection and the frequency of other types of diffracted radiation are close to each other, they are nonetheless different [see formula (24)], which allows the contributions of different types of radiation to be spectrally distinguished [43].

11. Results and discussion

The absolute values squared of the Fresnel coefficients for PXR (16), namely

$$|F_\perp|^2 = M\left|q_{\mathbf{g}\perp}(\omega_{\mathrm{PXR}})\right|^2 = \frac{M\pi^2\left|\chi_{\mathbf{g}}(\omega_{\mathrm{PXR}})\right|^2}{\left[c/(V\sqrt{\varepsilon}) - \cos\theta\right]^2}\,,$$
$$|F_\parallel|^2 = M\left|q_{\mathbf{g}\parallel}(\omega_{\mathrm{PXR}})\right|^2 = \frac{M\pi^2\left|\chi_{\mathbf{g}}(\omega_{\mathrm{PXR}})\right|^2 \cos^2(2\phi)}{\left[c/(V\sqrt{\varepsilon}) - \cos\theta\right]^2}\,, \tag{36}$$

coincide with expressions (12) obtained in paper [27] up to the factor of $\varepsilon^{7/2}(V/c)^2 \approx 1$ that has been discussed in Section 8. The expressions in the cited article correspond to the coefficients for the transformation of virtual photons into real ones, and they are in good agreement with the experimental data on the PXR reflection yield.

The values of the transformation coefficients (36) for typical experimental cases, presented in paper [27], have the order of 10^{-4} for low-index crystallographic planes of a silicon single-crystal. It may seem that the transformation coefficients (36) can be enhanced by increasing the number M of crystallographic planes — that is, the thickness of the crystal. Unfortunately, the effective number M is limited by the attenuation of the radiation in the crystal [see formula (18)]. Obviously, the phases of the Fresnel coefficients could not be obtained from the experimental data on the PXR yield in paper [27] due to the well-known 'phase problem' of the structure analysis [15]. Meanwhile, if the phases of the Fresnel coefficients are known, it allows, for example, easily determining the polarization structure of the PXR reflection discussed above.

In the present paper, the expressions for the angular distributions of the radiation yield and polarization in the PXR reflection were obtained in the first-order approximation in the angle of deflection from the reflection center. The higher-order considerations, performed in Refs [34, 44], show that the expressions for the angular distributions of the yield and the linear polarization directions in the PXR reflection, which is emitted perpendicularly to the particle beam at the angle $2\phi = \pi/2$, are slightly different from expressions (17), (22) and have new singularities. However, as far as we know, there have not yet been any experimental investigations of the properties such a reflection that would be accurate enough for a comparison of the results of both calculations to be performed.

The estimates presented above show that the conditions for PXR dynamic diffraction to be pronounced can be fulfilled in the crystals considered only for some low-index crystallographic planes in the central angular region of the PXR reflection, where the PXR yield is weak and can be masked by other types of radiation produced by the particle. Therefore, the influence of this phenomenon on the experimentally observed radiation yield in the PXR reflection is not high, and the basic properties of the radiation in the PXR reflection are well described by the kinematic theory. This does not exclude the possibility for some part of the radiation from the PXR reflection central region being diffracted in the forward direction, which is confirmed by the observations in papers [41, 42].

In the present paper, we have discussed the properties of the PXR generated from a straight (not bent) crystal. However, these properties can change dramatically in the case of PXR generation in a bent crystal. For example, one can focus the PXR emitted by a particle, which moves in a channeling regime through the bent crystal [25]. Moreover, the radiation in the PXR reflection maximum, after propagating along some path in the crystal, can be found in the conditions favorable for the dynamic diffraction due to the crystal curvature (see the example presented in Ref. [26]). However, PXR generated from a bent crystal has been poorly studied.

PXR occurs due to the interaction of the incident particle field with the electronic subsystem of the crystal. At the same time, coherent bremsstrahlung radiation is generated in the crystal due to the interaction of the particle with the nuclear subsystem of the crystal [6]. The periodicities of the electronic and nuclear subsystems in the crystal are, naturally, the same. Therefore, the frequencies of the spectral peaks of the coherent bremsstrahlung under the condition of $\hbar\omega \ll \gamma mc^2$ are described by the same formula (10) as the PXR frequency. The intensity maximum of the coherent bremsstrahlung is located in the angular region $\sim \gamma^{-1}$ around the particle's velocity vector $\mathbf{V}$, while the PXR reflection is usually emitted at a larger angle to the vector $\mathbf{V}$, and these two types of radiation do not influence each other. However, when the PXR reflection is emitted near the vector $\mathbf{V}$, their intensities can be of the same order and interference may occur. The interference of the PXR and the coherent bremsstrahlung was studied in papers [45–47].

All properties of PXR discussed above are independent of the charge sign of the incident particle. However, the phases of the radiation emitted by positively and negatively charged particles are opposite, and this may be important when PXR from electron–positron pairs is considered. The PXR yield (17) depends quadratically on the particle charge. This feature can be used for the experimental determination of the charge state of relativistic ions traveling through the crystal. Let us note that PXR is used to obtain both shadow and phase-contrast images (see, for example, paper [48]).

12. Conclusion

In the present paper, we have obtained analytical expressions of the Fresnel coefficients for PXR. We have also constructed the kinematic theory by using the Fresnel coefficients and

have shown that this theory can be applied to calculate basic properties of radiation in the PXR reflection.

It was shown that the calculated results for the basic observable properties of the PXR reflection, such as the frequency and width of the PXR spectral peak, as well as the fine structure of the PXR differential yield and the polarization, are in good agreement with the results of the kinematic theory [6], and with the experimental data on the PXR reflection found in the available literature.

Acknowledgments

The author is thankful to N F Shul'ga and A P Potylitsyn for the discussions regarding the report containing the main results of this paper at Xth International Symposium held in Armenia [49]. This paper was partially supported by the Ministry of Education and Science of the Russian Federation (project 3.2009.2014/K).

References

1. Born M, Wolf E *Principles of Optics* (Oxford: Pergamon Press, 1968); Translated into Russian: *Osnovy Optiki* (Moscow: Nauka, 1973)
2. Jackson J D *Classical Electrodynamics* (New York: Wiley, 1999)
3. Frank I M *Sov. Phys. Usp.* **8** 729 (1966); *Usp. Fiz. Nauk* **87** 189 (1965)
4. Ginzburg V L, Tsytovich V N *Phys. Rep.* **49** 1 (1979); *Usp. Fiz. Nauk* **126** 553 (1978)
5. Ginzburg V L, Tsytovich V N *Transition Radiation and Transition Scattering* (Bristol: A. Hilger, 1990); Translated from Russian: *Perekhodnoe Izluchenie i Perekhodnoe Rasseyanie* (Moscow: Nauka, 1984)
6. Ter-Mikaelian M L *High-Energy Electromagnetic Processes in Condensed Media* (New York: Wiley-Interscience, 1972); Translated from Russian: *Vliyanie Sredy na Elektromagnitnye Protsessy pri Vysokikh Energiyakh* (Erevan: Izd. AN Arm. SSR, 1969)
7. Ter-Mikaelian M L *Phys. Usp.* **44** 571 (2001); *Usp. Fiz. Nauk* **171** 597 (2001)
8. Fainberg Ya B, Khizhnyak N A *Sov. Phys. JETP* **5** 720 (1957); *Zh. Eksp. Teor. Fiz.* **32** 883 (1957)
9. Nitta H *Phys. Lett. A* **158** 270 (1991)
10. Shchagin A V, Maruyama X K, in *Accelerator-Based Atomic Physics: Techniques and Applications* (Eds S M Shafroth, J C Austin) (New York: AIP Press, 1997) p. 279
11. Potylitsyn A P *Electromagnetic Radiation of Electrons in Periodic Structures* (Heidelberg: Springer, 2011); Translated from Russian: *Izluchenie Elektronov v Periodicheskikh Strukturakh* (Tomsk: NTL, 2009)
12. Bazylev V A, Zhevago N K *Izluchenie Bystrykh Chastits v Veshchestve i vo Vneshnikh Polyakh* (Radiation of Fast Particles in Medium and in External Fields) (Moscow: Nauka, 1987)
13. Potylitsyn A P, Vnukov I E, in *Electron–Photon Interaction in Dense Media* (NATO Science Series, Ser. II, Vol. 49, Ed. H Wiedemann) (Dordrecht: Kluwer Acad. Publ., 2002) p. 25
14. Als-Nielsen J, McMorrow D *Elements of Modern X-ray Physics* 2nd ed. (Hoboken: Wiley, 2011)
15. Zhdanov G S, Ilyushin A S, Nikitina S V *Difraktsionnyi i Rezonansnyi Strukturnyi Analiz* (Diffractional and Resonant Structure Analysis) (Moscow: Nauka, 1980)
16. Pinsker Z G *Dynamical Scattering of X-Rays in Crystals* (New York: Springer, 1978); Translated from Russian: *Rentgenovskaya Kristallooptika* (Moscow: Nauka, 1982)
17. Shchagin A V *Radiation Phys. Chem.* **61** 283 (2001)
18. Shchagin A V, Khizhnyak N A *Nucl. Instrum. Meth. Phys. Res. B* **119** 115 (1996)
19. Shchagin A V, Pristupa V I, Khizhnyak N A *Phys. Lett. A* **148** 485 (1990)
20. Shchagin A V, in *Electron–Photon Interaction in Dense Media* (NATO Science Series, Ser. II, Vol. 49, Ed. H Wiedemann) (Dordrecht: Kluwer Acad. Publ., 2002) p. 133
21. Morokhovskii V L, Shchagin A V *Sov. Phys. Tech. Phys.* **35** 623 (1990); *Zh. Tekh. Fiz.* **60** (5) 147 (1990)
22. Shchagin A V *J. Phys. Conf. Ser.* **236** 012020 (2010)
23. Brenzinger K-H et al. *Phys. Rev. Lett.* **79** 2462 (1997)
24. Shul'ga N F, Tabrizi M *JETP Lett.* **76** 279 (2002); *Pis'ma Zh. Eksp. Teor. Fiz.* **76** 337 (2002)
25. Shchagin A V *JETP Lett.* **80** 469 (2004); *Pis'ma Zh. Eksp. Teor. Fiz.* **80** 535 (2004)
26. Shchagin A V, in *Advanced Radiation Sources and Applications* (NATO Science Series, Ser. II, Vol. 199, Ed. H Wiedemann) (Dordrecht: Springer, 2006) p. 27
27. Shchagin A V, Takabayashi Y *Nucl. Instrum. Meth. Phys. Res. B* **309** 198 (2013)
28. Brenzinger K-H et al. *Z. Phys. A* **358** 107 (1997)
29. Takabayashi Y, Shchagin A V *Nucl. Instrum. Meth. Phys. Res. B* **278** 78 (2012)
30. Shchagin A V, Pristupa V I, Khizhnyak N A *Nucl. Instrum. Meth. Phys. Res. B* **99** 277 (1995)
31. Sones B, Danon Y, Block R C *Nucl. Instrum. Meth. Phys. Res. B* **227** 22 (2005)
32. Fiorito R B et al. *Phys. Rev. E* **51** R2759 (1995)
33. Shchagin A V, Sotnikov V V *Voprosy Atom. Nauki Tekh. Ser. Plazmennaya Elektron. Novye Metody Uskoreniya* (4(6)) 316 (2008)
34. Shchagin A V *Phys. Lett. A* **247** 27 (1998)
35. Morokhovskii V V et al. *Phys. Rev. Lett.* **79** 4389 (1997)
36. Baryshevskii V G, Feranchuk I D *Sov. Phys. JETP* **34** 502 (1972); *Zh. Eksp. Teor. Fiz.* **61** 994 (1971)
37. Garibian G M, Yang C *Sov. Phys. JETP* **34** 495 (1972); *Zh. Eksp. Teor. Fiz.* **61** 930 (1971)
38. Baryshevsky V G *Nucl. Instrum. Meth. Phys. Res. B* **122** 13 (1997)
39. Artru X, Rullhusen P *Nucl. Instrum. Meth. Phys. Res. B* **145** 1 (1998); addendum: *Nucl. Instrum. Meth. Phys. Res. B* **173** 16 (2001)
40. Nitta H *J. Phys. Soc. Jpn.* **69** 3462 (2000)
41. Backe H et al. *Nucl. Instrum. Meth. Phys. Res. B* **234** 138 (2005)
42. Aleinik A N et al. *JETP Lett.* **80** 339 (2004); *Pis'ma Zh. Eksp. Teor. Fiz.* **80** 447 (2004)
43. Shchagin A V *Vestn. Kharkov. Nats. Univ. Ser. Fiz. Yadra, Chastitsy, Polya* (3(39)) 91 (2008)
44. Shchagin A V *Phys. Lett. A* **262** 383 (1999)
45. Blazhevich S V et al. *Phys. Lett. A* **195** 210 (1994)
46. Kleiner V L, Nasonov N N, Safronov A G *Phys. Status Solidi B* **181** 223 (1994)
47. Morokhovskyi V V et al. *Phys. Rev. B* **61** 3347 (2000)
48. Hayakawa Y et al. *JINST* **8** C08001 (2013)
49. Shchagin A V, in *X Intern. Symp. Radiation from Relativistic Electrons in Periodic Structures, Lake Sevan, Armenia, September 23–28, 2013* Book of Abstracts (Tomsk: Tomsk Polytechnic Univ. Publ. House, 2013) p. 49